Existence, stability and dynamics of solitary waves in spinor dynamical lattices

2010 J. Phys. A: Math. Theor. 43 505203

(http://iopscience.iop.org/1751-8121/43/50/505203)

IOP PUBLISHING JOURNAL OF PHYSICS A: MATHEMATICAL AND THEORETICAL

J. Phys. A: Math. Theor. **43** (2010) 505203 (16pp) doi:10.1088/1751-8113/43/50/505203

Existence, stability and dynamics of solitary waves in spinor dynamical lattices

Z Shi[1], H Susanto[2], R L Horne[3], N Whitaker[1] and P G Kevrekidis[1]

[1] Department of Mathematics and Statistics, University of Massachusetts, Amherst, MA 01003-4515, USA
[2] School of Mathematical Sciences, University of Nottingham, University Park, Nottingham NG7 2RD, UK
[3] Department of Mathematics, Morehouse College, Atlanta, GA 30314, USA

E-mail: kevrekid@math.umass.edu

Received 8 June 2010, in final form 4 October 2010
Published 23 November 2010
Online at stacks.iop.org/JPhysA/43/505203

Abstract

In this work, motivated by the context of spinor ($F = 1$) Bose–Einstein condensates that can be described by a quasi-one-dimensional model, we examine three-component dynamical lattices which feature the mean-field nonlinearity of the spinor system. Starting at the anti-continuum limit of uncoupled lattice sites, we develop a systematic perturbative approach of the types of modes that can emerge, depending on the relative phase of the excited sites. We examine one-, two- and three-excited site states, offer a systematic analysis of their linear stability and observe typical manifestations of the corresponding instabilities, when the lattice coherent structures are found to be linearly unstable. Despite the significantly different eigenvalue count, interestingly, we find that in the configurations examined the principal stability features remain similar to the single-component dynamical lattice in the immediate vicinity of the anti-continuum limit.

PACS numbers: 03.75.Lm, 03.75.Mn
Mathematics Subject Classification: 35Q55, 37K45, 37K50

(Some figures in this article are in colour only in the electronic version)

1. Introduction

One of the particularly interesting new directions in the study of Bose–Einstein condensates (BECs) has been the development of far-off-resonant optical techniques for trapping of ultracold atomic gases. This has enabled the confinement of atoms regardless of their spin (hyperfine) state, see e.g. [1]. In turn, this has led to the experimental creation of *spinor*

BECs [2, 3], in which the spin degree of freedom (frozen in magnetic traps) becomes relevant. Various phenomena that are not present in single-component BECs, including formation of spin domains [4] and spin textures [5], emerge in this setting.

In the case of a spinor condensate formed by atoms with spin F, the relevant mean-field description involves a $(2F + 1)$-component macroscopic wavefunction. Accordingly, a number of theoretical works have been dealing with multi-component (*vector*) solitons in $F = 1$ spinor BECs. Bright [6–8] and dark [9] solitons have been predicted in this setting, including compound solitons which are bright in some components but dark in others [10], as well as vortices and vortex lattices in higher dimensions [11]. More relevant to the context of the present work, different types of solitary waves have also been predicted in the context of optical lattices, such as gap solitons [12], interacting dark solitons [13], sine-Gordon-type solitons in the presence of optical lattices and dipolar interactions [14] and many others. Interestingly, recent experiments in these systems have been able to not only unveil interesting magnetic pattern phenomena [15] but also place the system within optical lattices even without the typical square symmetry—namely in the triangular optical lattices of [16].

This motivates the question of the dynamics of spinor condensates in such optical lattice systems and whether we can understand its features, not only numerically but also from a tractable analytical limit. This is the context of our present work. In particular, we are motivated by the continuum model of the spinor condensates in the presence of an optical lattice and by its analogy (in the context of deep lattices) to a dynamical lattice model with the same ('onsite') nonlinear terms, to explore the corresponding lattice model. This analogy can be made rigorous in a spirit similar to that of [17] for the single-component problem. More specifically, a Wannier function expansion can be used to convert the problem with the (deep) periodic potential into a lattice problem, whereby the linear part of the operator translates into a linear (tunneling) coupling between adjacent wells, while the dominant contribution to the nonlinearity stems from the 'onsite' terms. Our exploration commences with this lattice model at the so-called anti-continuum limit where adjacent sites are uncoupled with each other and hence the resulting ordinary differential equations (ODEs) can be solved explicitly. Subsequently, upon exciting one or a few (herein we examine excitation of up to three) of these sites, we examine which of the relevant structures could be sustained at finite coupling (i.e. tunneling rate) and what their corresponding stability is. One of the advantages of the perturbative approach from the uncoupled limit is that explicit analytical expressions can be developed to approximate both the relevant solutions' spatial structure and, importantly, their corresponding eigenvalues. These are indicative of which among these structures we should expect to be stable at intermediate (or large) values of the coupling, where the model may be physically relevant as an approximation of the superfluid regime of a spinor condensate within an optical lattice. One of the interesting conclusions emerging from our work is that the principal stability features of the multi-site structure resemble those of the considerably simpler single-component discrete nonlinear Schrödinger (DNLS) problem, at least in the vicinity of the anti-continuum limit; for the latter, see the discussion of [18, 19]. It should be noted, however, that this conclusion is not necessarily and generally true for arbitrary values of the coupling.

The presentation of our results is hereafter structured as follows. In section 2, we formulate the general theoretical setup of our study. In section 3, we present our analytical considerations for the various coherent structures and their corresponding stability results. In section 4, we explore the validity of these predictions against detailed numerical investigations of the relevant modes. Finally, in section 5, we summarize our findings and present some directions for future work.

2. Theoretical setup

The theoretical formulation of the problem that we will use herein is a lattice analog of the one used in [12], which reads[4]

$$\mathrm{i}\partial_t \psi_{\pm 1,n} = \epsilon \Delta \psi_{\pm 1,n} + \nu_s S \psi_{\pm 1,n} + \nu_a (S - 2|\psi_{\mp 1,n}|^2)\psi_{\pm 1,n} + \nu_a \psi_{0,n}^2 \psi_{\mp 1,n}^* \quad (1)$$

$$\mathrm{i}\partial_t \psi_{0,n} = \epsilon \Delta \psi_{0,n} + \nu_s S \psi_{0,n} + \nu_a (S - |\psi_{0,n}|^2)\psi_{0,n} + 2\nu_a \psi_{0,n}^* \psi_{1,n} \psi_{-1,n}. \quad (2)$$

In these expressions $S = |\psi_{-1,n}|^2 + |\psi_{0,n}|^2 + |\psi_{1,n}|^2$ represents the total normalized density, while the coupling coefficients ν_s and ν_a represent, respectively, the symmetric spin-independent and the antisymmetric spin-dependent interaction strengths, which in the following we take to be $\nu_s = 1$ and $\nu_a = r$. Additionally, the discrete Laplacian reads

$$\Delta \psi_{j,n} = \psi_{j,n+1} - 2\psi_{j,n} + \psi_{j,n-1}, \quad (3)$$

where $j = -1, 0, 1$.

We now seek stationary solutions of equations (1) and (2) in the form $\psi_{j,n} = u_{j,n} \exp(-\mathrm{i}\mu_j t) \exp(\mathrm{i}\theta_j)$, where μ_j and θ_j correspond, respectively, to the chemical potentials and phases of the wavefunctions. This ansatz results in the following equations for the stationary states $u_{j,n}$:

$$F_{\pm 1,n} := -\mu_{\pm 1} u_{\pm 1,n} + \epsilon \Delta u_{\pm 1,n} + S u_{\pm 1,n} + r(S - 2|u_{\mp 1,n}|^2)u_{\pm 1,n} + p r u_{0,n}^2 u_{\mp 1,n}^* = 0, \quad (4)$$

$$F_{0,n} := -\mu_0 u_{0,n} + \epsilon \Delta u_{0,n} + S u_{0,n} + r(S - |u_{0,n}|^2)u_{0,n} + 2 p r u_{0,n}^* u_{1,n} u_{-1,n} = 0, \quad (5)$$

where $p = \exp(\mathrm{i}(\theta_{+1} + \theta_{-1} - 2\theta_0))$. The chemical potentials and phases have to obey the usual constraints [12]

$$2\mu_0 = \mu_1 + \mu_{-1}, \theta_1 + \theta_{-1} - 2\theta_0 = n\pi,$$

which are the so-called phase matching conditions relevant for stationary states typically in systems with parametric interactions.

When $\mu_0 \neq \mu_{-1} \neq \mu_{+1}$, $\Pi_{j=-1}^{1} u_{j,n} = 0$. Therefore, in the following we consider $\mu_j = \mu$. Nontrivial solutions to (4) and (5) when $\epsilon = 0$ are then given by the following conditions for the solution amplitudes $u_+ = A$, $u_0 = B$ and $u_- = C$:

(I.1) $p = 1$, $A = -C$, $B = \pm\sqrt{\mu - 2C^2}$, where $|C| < \sqrt{\mu/2}$;
(I.2) $p = 1$, $A = \sqrt{\mu/(1+r)} - C$, $B = \pm\sqrt{2AC}$, where $\sqrt{\mu/(1+r)} \geqslant C \geqslant 0$;
(I.3) $p = 1$, $A = -\sqrt{\mu/(1+r)} - C$, $B = \pm\sqrt{2AC}$, where $-\sqrt{\mu/(1+r)} \leqslant C \leqslant 0$;

(II.1) $p = -1$, $A = C$, $B = \pm\sqrt{\mu - 2C^2}$, where $|C| < \sqrt{\mu/2}$;
(II.2) $p = -1$, $A = \sqrt{\mu/(1+r)} + C$, $B = \pm\sqrt{-2AC}$, where $-\sqrt{\mu/(1+r)} \leqslant C \leqslant 0$;
(II.3) $p = -1$, $A = -\sqrt{\mu/(1+r)} + C$, $B = \pm\sqrt{-2AC}$, where $\sqrt{\mu/(1+r)} \geqslant C \geqslant 0$.

Note that A and B depend on C, which is a free parameter. The chemical potential μ does not uniquely determine C, but rather allows to estimate a bound for it. These results for $\epsilon = 0$ are the starting point of our analysis of the solutions, $U_{j,n}$, for finite ϵ. In particular, upon calculating the solutions at $\epsilon = 0$, we continue them to finite coupling by varying ϵ for different values of the other parameters. The excited sites at $\epsilon = 0$ are given by the above expressions, among which in the following we use either (I.2) or (I.3) because these are the

[4] It should be noted, however, that for notational simplicity here we use the focusing formulation of the equations of motion; for the defocusing case, the sign of ϵ can be negative, or equivalently one can use the well-known staggering transformation $\Psi_{i,n} = (-1)^n \psi_{i,n}$ which changes the conclusions (including the stability ones) for in-phase configurations below to those for out-of-phase ones and vice versa.

only genuine three-distinct-component solutions of the system in the case of $p = 1$. Similar conclusions can be extracted (to the ones below) for the case of $p = -1$ for the solutions (II.2) and (II.3).

The stability of any given solution $U_{j,n}$ is determined by writing

$$\psi_{j,n}(t) = \mathrm{e}^{\mathrm{i}\mu t}[U_{j,n} + (x_{j,n} + \mathrm{i}y_{j,n})\,\mathrm{e}^{\lambda t} + (x^*_{j,n} + \mathrm{i}y^*_{j,n})\,\mathrm{e}^{\lambda^* t}], \tag{6}$$

where $x_{j,n}$ and $y_{j,n}$ are the small perturbations. Substituting the perturbed solution into the governing equations will lead to the linear stability system

$$\mathcal{M}\begin{pmatrix} \vdots \\ X_{-1} \\ X_0 \\ X_1 \\ \vdots \end{pmatrix} = -\Omega\begin{pmatrix} \vdots \\ X_{-1} \\ X_0 \\ X_1 \\ \vdots \end{pmatrix}, \tag{7}$$

where

$$\mathcal{M} = \begin{pmatrix} \ddots & \ddots & \ddots & & & & \\ & M_\epsilon & M^-_{-1} & M_\epsilon & & & \\ & & M_\epsilon & M^-_0 & M_\epsilon & & \\ & & & M_\epsilon & M^-_1 & M_\epsilon & \\ & & & & \ddots & \ddots & \ddots \end{pmatrix} \times \begin{pmatrix} \ddots & \ddots & \ddots & & & & \\ & M_\epsilon & M^+_{-1} & M_\epsilon & & & \\ & & M_\epsilon & M^+_0 & M_\epsilon & & \\ & & & M_\epsilon & M^+_1 & M_\epsilon & \\ & & & & \ddots & \ddots & \ddots \end{pmatrix},$$

$M_\epsilon = \mathrm{diag}(\epsilon, \epsilon, \epsilon)$, $\Omega = \lambda^2$ and $X_n = (x_{-1,n},\ x_{0,n},\ x_{1,n})^T$. The matrix component at row k and column l, $k, l = 1, 2, 3$, of $M^\pm_n$ is given by

$$M^\pm_{n,k,l} = \left(\frac{\partial F_{(k-2),n}}{\partial u_{(l-2),n}} \pm \frac{\partial F_{(k-2),n}}{\partial u^*_{(l-2),n}}\right)\Bigg|_{U_{j,n}, j=-1,0,1}.$$

3. Analytical calculations

In this subsection, we attempt to study the existence and stability of localized modes analytically, where we will use perturbation analysis as described e.g. in [18]. The method is based on the expansion in the coupling constant ϵ in the vicinity of the anti-continuum limit. Therefore, we write all variables in a power series of ϵ, which up to $\mathcal{O}(\epsilon^2)$ can be expressed as

$$U_{j,n} = U^{(0)}_{j,n} + \epsilon U^{(1)}_{j,n}, \qquad \mathcal{M} = \mathcal{M}^{(0)} + \epsilon\mathcal{M}^{(1)},$$
$$\mathbf{X} = \mathbf{X}^{(0)} + \epsilon\mathbf{X}^{(1)}, \qquad \Omega = \Omega^{(0)} + \epsilon\Omega^{(1)}.$$

It can be checked that $\mathcal{M}^{(0)}$ is a singular self-adjoint matrix.

In the limit of $\epsilon = 0$, there are two types of solutions, i.e. $u_{j,n} = 0$ and the non-zero solutions which, as indicated above, herein are of the form (I.2) or (I.3). In this limit, one

can also easily note that the eigenvalue problem (7) will give $\lambda = \pm i\mu$ for the sites associated with the zero (i.e. trivial) solutions and

$$\lambda = \pm 0, \qquad \pm i\frac{2\mu r}{1+r} \tag{8}$$

for the sites associated with non-zero solutions.

It can be directly inferred from the analysis of the underlying linear problem that the stable eigenvalues $\lambda = \pm i\mu$ will expand, creating a band of continuous spectrum when ϵ is increased. Therefore, this eigenvalue (of infinite multiplicity, when $\epsilon = 0$) will not be discussed further. The potential instability for a soliton solution will then be determined by the bifurcation of the remaining eigenvalues. Especially important in that regard are the eigenvalues at the origin which may *immediately* lead to instability, as soon as ϵ deviates from the anti-continuum limit. Analytically this bifurcation will be calculated using perturbation analysis.

To illustrate our method, let us first consider the profile of intersite modes, i.e. $\ldots 00 + +00 \ldots$. This notation will be taken to mean that at $\epsilon = 0$, the mode is given by

$$U^{(0)}_{-1,n} = \begin{cases} C, & n = 0, 1, \\ 0, & n \text{ elsewhere} \end{cases},$$

$$U^{(0)}_{1,n} = \begin{cases} \sqrt{\mu/(1+r)} - C, & n = 0, 1, \\ 0, & n \text{ elsewhere} \end{cases},$$

$$U^{(0)}_{0,n} = \begin{cases} \sqrt{2U^{(0)}_{1,n}U^{(0)}_{-1,n}}, & n = 0, 1, \\ 0, & n \text{ elsewhere.} \end{cases}$$

It is clear that for finite ϵ, the solutions will be deformed from their uncoupled limit profile. The correction $U^{(1)}_{j,n}$ can be found from equations at $\mathcal{O}(\epsilon)$ of (4) and (5), which due to their lengthy expressions are not presented here.

The next step is to consider the stability problem when the coupling is turned on. To leading order, the eigenvalue problem of this particular configuration is given by

$$\mathcal{M}^{(0)}_A \mathbf{X}^{(0)} = -\Omega^{(0)}\mathbf{X}^{(0)}, \tag{9}$$

where

$$\mathcal{M}_A = \begin{pmatrix} M_0^- & M_\epsilon \\ M_\epsilon & M_1^- \end{pmatrix}\begin{pmatrix} M_0^+ & M_\epsilon \\ M_\epsilon & M_1^+ \end{pmatrix} = \mathcal{M}^{(0)}_A + \epsilon\mathcal{M}^{(1)}_A + \cdots,$$

from which one will obtain that Ω_0 is the square of the eigenvalues of equation (8).

First, let us consider the eigenvalue $\Omega^{(0)} = 0$ which is of multiplicity four, with corresponding eigenvectors denoted by e_k, $k = 1, \ldots, 4$. Hence, one can write the leading-order eigenvector

$$\mathbf{X}^{(0)} = \sum_{k=1}^{4} c_k e_k.$$

The next-order equation of the eigenvalue problem is

$$\mathcal{M}^{(0)}_A \mathbf{X}^{(1)} + \mathcal{M}^{(1)}_A \mathbf{X}^{(0)} = -\Omega^{(1)}\mathbf{X}^{(0)}. \tag{10}$$

Projecting the equation above to e_j, $j = 1, \ldots, 4$, i.e. basis of the null space of $\mathcal{M}^{(0)}_A$, will give us the following generalized eigenvalue problem:

$$\Xi_L \begin{pmatrix} c_1 \\ c_2 \\ c_3 \\ c_4 \end{pmatrix} = -\Omega^{(1)}\,\Xi_R \begin{pmatrix} c_1 \\ c_2 \\ c_3 \\ c_4 \end{pmatrix}, \tag{11}$$

where Ξ_L and Ξ_R are the 4×4 coefficient matrices. The system can be immediately solved to yield $\Omega^{(1)} = 4\mu$, and $\Omega^{(1)} = 0$ with multiplicity three. This illustrates that there is a pair of eigenvalues bifurcating from zero given by

$$\lambda = \pm 2\sqrt{\mu}\sqrt{\epsilon} + \mathcal{O}(\epsilon). \tag{12}$$

Taking the same calculations to the non-zero eigenvalues of (8), i.e. $\Omega^{(0)} = -4\mu^2 r^2/(1+r)^2$, will yield that $\Omega^{(1)} = \frac{-8\mu r^2}{(1+r)^2}, \frac{-8\mu r(1+2r)}{(1+r)^2}$. This informs us that there are two stable, bifurcating eigenvalues given by

$$\lambda = \pm \mathrm{i}\frac{2\mu r + 2r\epsilon}{1+r}, \qquad \pm \mathrm{i}\frac{2\mu r + (2+4r)\epsilon}{1+r}. \tag{13}$$

The same procedure can be applied to bifurcations of zero eigenvalues of twisted modes, i.e. $\ldots 00 + -00 \ldots$. Once again, this notation is taken to imply that at $\epsilon = 0$, the mode is given by

$$U^{(0)}_{-1,n} = \begin{cases} C, & n = 0, \\ -C, & n = 1, \\ 0, & n \text{ elsewhere}, \end{cases}$$

$$U^{(0)}_{1,n} = \begin{cases} \sqrt{\mu/(1+r)} - C, & n = 0, \\ -\sqrt{\mu/(1+r)} + C, & n = 1, \\ 0, & n \text{ elsewhere}, \end{cases}$$

$$U^{(0)}_{0,n} = \begin{cases} \sqrt{2U^{(0)}_{1,n}U^{(0)}_{-1,n}}, & n = 0, \\ -\sqrt{2U^{(0)}_{1,n}U^{(0)}_{-1,n}}, & n = 1, \\ 0, & n \text{ elsewhere}. \end{cases}$$

The above procedure can be similarly and immediately applied to this twisted configuration to obtain the bifurcating eigenvalues

$$\lambda = \pm \mathrm{i}2\sqrt{\mu}\sqrt{\epsilon}, \qquad \pm \mathrm{i}\frac{2\mu r + 6r\epsilon}{1+r}, \qquad \pm \mathrm{i}\frac{2\mu r + 2(-1+2r)\epsilon}{1+r}. \tag{14}$$

For three-excited-site modes, the same procedure will give us

$$\begin{aligned} &\lambda = \pm\sqrt{2\mu}\sqrt{\epsilon}, \qquad \pm\sqrt{6\mu}\sqrt{\epsilon}, \qquad \pm \mathrm{i}\frac{2\mu r + (3r+1)\epsilon}{1+r}, \\ &\pm \mathrm{i}\frac{4\mu r + (3 + 5r \pm \sqrt{9r^2 + 14r + 9})\epsilon}{2(1+r)}, \end{aligned} \tag{15}$$

in the case of the three in-phase excited-site configuration $\ldots 00 + + + 00 \ldots$. On the other hand, the process yields the eigenvalues

$$\lambda = \sqrt{\pm 2\sqrt{3}\mu}\sqrt{\epsilon}, \qquad \pm \mathrm{i}\frac{2\mu r + 4r\epsilon}{1+r}, \qquad \pm \mathrm{i}\frac{2\mu r + (4r \pm \sqrt{3r^2 + 2r + 3})\epsilon}{1+r} \tag{16}$$

for the case of the $\ldots 00 + + - 00 \ldots$ configuration, and

$$\begin{aligned} &\lambda = \pm \mathrm{i}\sqrt{2\mu}\sqrt{\epsilon}, \qquad \pm \mathrm{i}\sqrt{6\mu}\sqrt{\epsilon}, \qquad \pm \mathrm{i}\frac{2\mu r + (5r-1)\epsilon}{1+r}, \\ &\pm \mathrm{i}\frac{4\mu r + (-3 + 11r \pm \sqrt{9r^2 + 14r + 9})\epsilon}{2(1+r)} \end{aligned} \tag{17}$$

for the $\ldots 00 + - + 00 \ldots$ coherent state.

A remarkable observation regarding the above results is that despite the differences of the spinor discrete model with the standard single-component DNLS model, the former preserves

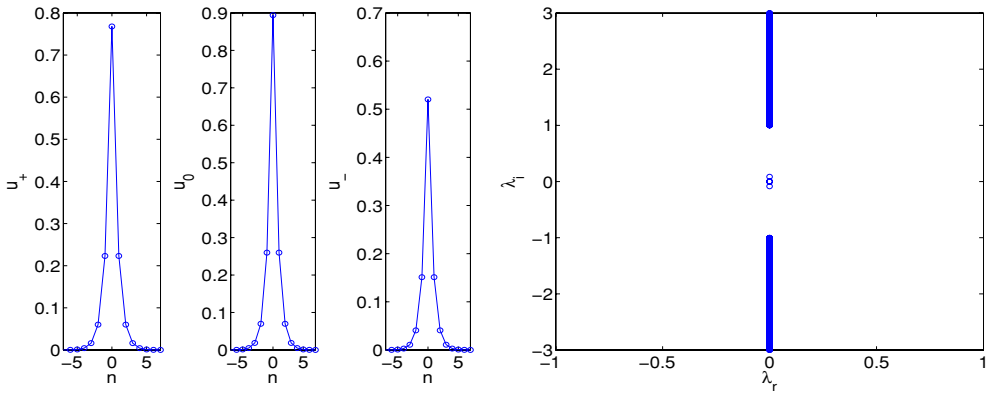

Figure 1. The left panel shows the spatial profile of the three components for the numerically exact discrete spinor solution on the lattice for $\epsilon = 0.5$ and $\mu = 1$. The right panel shows the spectral plane (λ_r, λ_i) of the linearization eigenvalues $\lambda = \lambda_r + \mathrm{i}\lambda_i$. The absence of eigenvalues with a non-zero real part illustrates the stability of the considered state. $C = 0.4$ was used here and in the results that follow.

the eigenvalue pairs that the latter possessed as well; compare with the results of [18]. In addition to these eigenvalues which are responsible for the instability of configurations with in-phase neighbors (and the linear stability of states with purely out-of-phase neighbors for small ϵ), the spinor system appears to have some eigenvalues that depend on μ, ϵ and r but in a 'benign' way at least for small ϵ. Hence, we chiefly observe in the spinor system the same instabilities as in the single-component DNLS model, a result which can certainly not be expected *a priori*. Additionally, we should note here that while we considered configurations that are similar in their spatial structure across components (e.g. in-phase in all components, or out-of-phase in all of them), it is, in principle, possible to also consider the so-called mixed states. In the latter setting, an in-phase configuration in one of the components is coupled to an out-of-phase configuration in another one among them. Although we considered such configurations in our numerical computations, we were unable to continue them even for relatively small values of the coupling past the anti-continuum limit. For this reason, we will not consider them further herein.

4. Numerical results

We now turn to a systematic numerical investigation of the various one-, two- and three-excited-site structures.

4.1. Single-excited-site waveform . . . 00 + 00 . . .

The single-site structure has only a single eigenvalue pair at the origin of the spectral plane. As ϵ increases, this eigenvalue will remain at the origin due to the single preserved gauge invariance (associated with the conservation of the total norm $\sum_{n,j} |\psi_{j,n}|^2$). In addition, the double pair at $\pm 2\mathrm{i}\mu r/(1 + r)$ will move by an amount proportional to ϵ, but without causing an instability to this fundamental soliton structure. This structure is expected to persist at *all* values of ϵ and gradually shape itself as a bright soliton of the full spinor system in the continuum limit of $\epsilon \to \infty$. A typical example of this state and of its linear stability for $\epsilon = 0.5$ is shown in figure 1. For this Hamiltonian system, the eigenvalues $\lambda = \lambda_r + \mathrm{i}\lambda_i$ bear

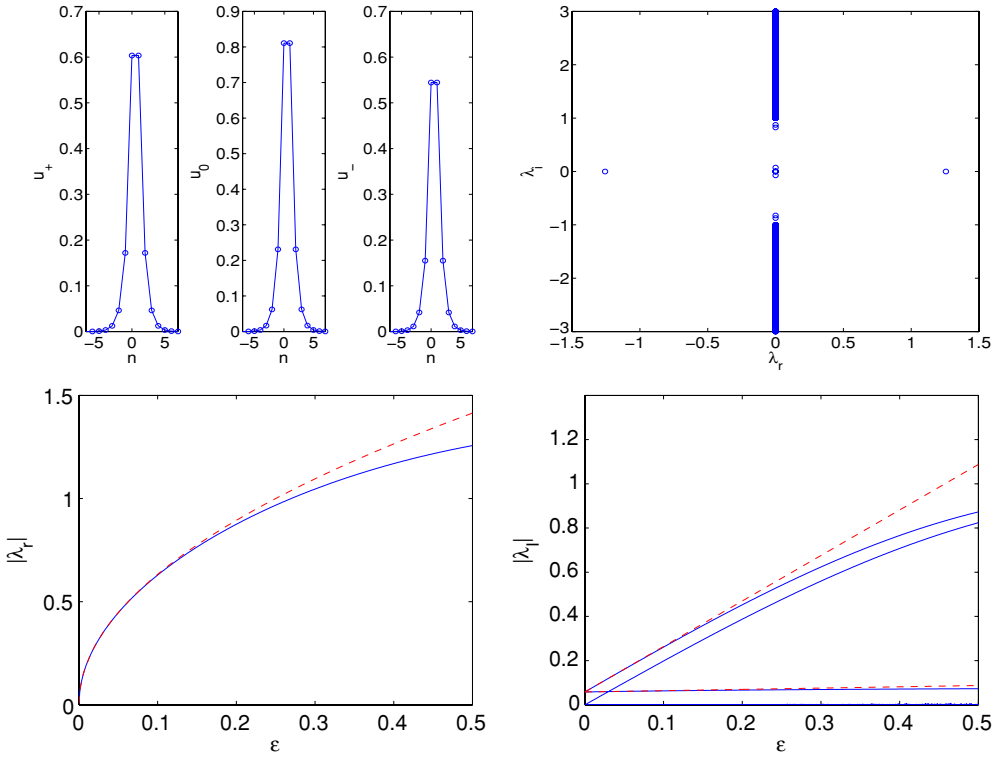

Figure 2. The top panels show a typical profile of the two-site, in-phase $\ldots 00 + +00 \ldots$ mode (left) and its corresponding linearization spectrum in the case of $\epsilon = 0.5$ (right). The bottom-left panel shows the real eigenvalue for small ϵ as predicted by equation (12) (dashed line), compared with the direct numerical results (solid line). The bottom-right panel shows a similar comparison between the imaginary eigenvalues predicted by equation (13) (dashed lines) and the full numerical result (solid lines).

the symmetry that if λ is an eigenvalue, then so are $-\lambda$, λ^* and $-\lambda^*$; hence, the absence of any eigenvalue with a non-zero real part (i.e. the presence of all eigenvalues on the imaginary axis) is tantamount to the spectral stability of the system.

4.2. Two in-phase excited-site waveform $\ldots 00 + +00 \ldots$

We now turn to the two-site solutions, starting from the in-phase configuration of the form $\ldots 00{+}{+}00 \ldots$. In this case, as predicted by equation (12), we expect the configuration to bear a real eigenvalue which is indeed the case as shown in figure 2 (bottom-left panel). A typical configuration of this form, again for $\epsilon = 0.5$, and its linear (in)stability are shown in the figure, as are the relevant imaginary eigenvalues, which are found to be in very good agreement with the predictions of equation (13) for the two modes bifurcating off of $\lambda = \pm 2\mathrm{i}\mu r/(1 + r)$ (at $\epsilon = 0$). It should be noted that, while unstable, this configuration is also expected to persist at arbitrary values of the coupling ϵ, all the way to the continuum limit of $\epsilon \to \infty$. In that limit, and upon the restoration of the translational invariance responsible for the instability of this intersite solution [19], it converges to the same (stable) continuum limit as the $\ldots 00 + 00 \ldots$ mode.

We also examined the typical dynamics of the evolution of this unstable spinor pattern. A relevant example for the case of $\epsilon = 0.5$ is shown in figure 3. It can be seen that after

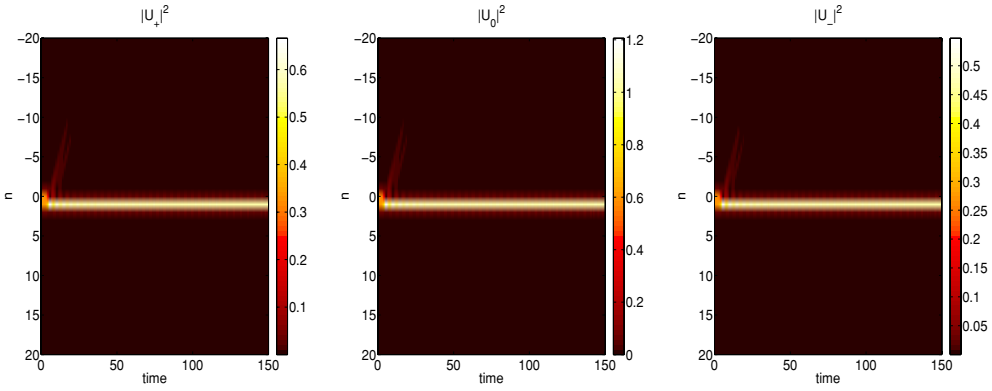

Figure 3. Spacetime contour plots of the density $|\psi_{j,n}|^2$ for the fields with $j = 1$ (left), $j = 0$ (middle) and $j = -1$ (right) for $\epsilon = 0.5$. The evolution clearly shows the deformation of the state into a single-site mode.

a relatively short time interval, the large growth rate of the instability contributes to the destabilization and eventual transformation of the solution into a single-site-type state which is stable and persists for much longer dynamical evolutions.

4.3. Two out-of-phase excited-site waveform $\ldots 00+-00\ldots$

We now turn to the case of the out-of-phase waveform $\ldots 00+-00\ldots$ for all three components. In this case, we find that the configuration is stable for small ϵ in accordance with the analytical prediction and becomes unstable for $\epsilon > 0.147$. In fact, we are unable to continue such solutions past $\epsilon \approx 0.77$. This is natural as such solutions do not exist (as stationary states) in the continuum limit of the system. In figure 4, we show some typical examples of this profile such as the stable case of $\epsilon = 0.1$ and the unstable one of $\epsilon = 0.2$. In the latter one, an oscillatory instability has set in due to the collision of a negative Krein signature imaginary eigenvalue pair (bifurcating from the origin as ϵ becomes non-zero) with the band edge of the continuous spectrum of the problem at $\pm i\mu$ (here $\mu = 1$). The dependence of the relevant imaginary eigenvalues (as well as of the real part of the emerging unstable quartet) is also shown in the figure and is compared to the theoretical prediction of equation (14).

Subsequently, we illustrate the unstable evolution of the density of the three spinor components for the unstable case of $\epsilon = 0.2$ shown in figure 4. The contour plot of the evolution in figure 5 showcases the fact that the dynamics upon an oscillatory growth eventually reshapes itself into a single-site excitation. It is worth noting here that the instability evolution is considerably slower than the dynamics of, say, figure 3 due to the much smaller growth rate of the complex eigenmode of the present setting in comparison to the real eigenvalue of the latter.

4.4. Three in-phase excited-site waveform $\ldots 00+++00\ldots$

We now turn to excitations involving three sites at the anti-continuum limit, starting from the in-phase structure of the form $\ldots 00+++00\ldots$ for all three components. The relevant solution is unstable for all the considered positive values of ϵ, due to two real eigenvalue pairs, in agreement with the theoretical prediction. It is worth noting that these eigenvalue pairs are very accurately predicted by the theoretical expressions of equation (15) for small values of ϵ. However, for $\epsilon > 0.1$, this prediction becomes progressively inadequate essentially due to

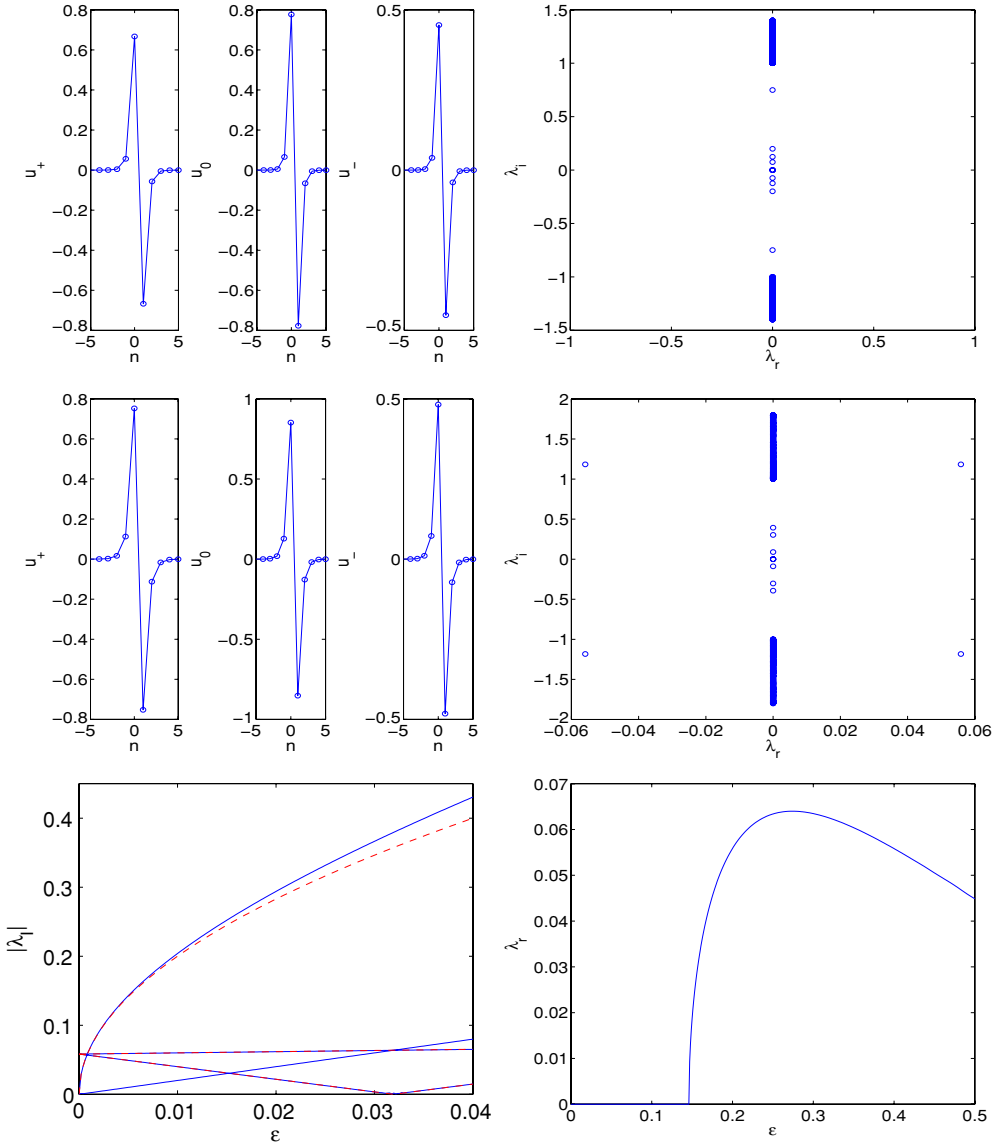

Figure 4. The top and middle rows of panels show the out-of-phase configurations and their corresponding spectral plane, similarly to, e.g., figure 2, for the stable case of $\epsilon = 0.1$ and the oscillatorily unstable one of $\epsilon = 0.2$, respectively. The bottom panel explores the dependence of the relevant eigenvalues on ϵ. This is done for the imaginary ones, which numerically (solid lines) are found to be in excellent agreement with the theoretical prediction of equation (14) (dashed lines), in the left panel and for the real part of the instability-inducing quartet in the right panel.

the significant contribution of higher order terms in the solution and eigenvalue expansions. Figure 6 illustrates the relevant solution and its stability for $\epsilon = 0.3$. The profile shown in the figure can be continued up to $\epsilon = 0.374$.

The density evolution of the static profile presented in figure 6 is shown in figure 7. Here, we can observe the strong instability of the in-phase, three-site branch giving rise to its

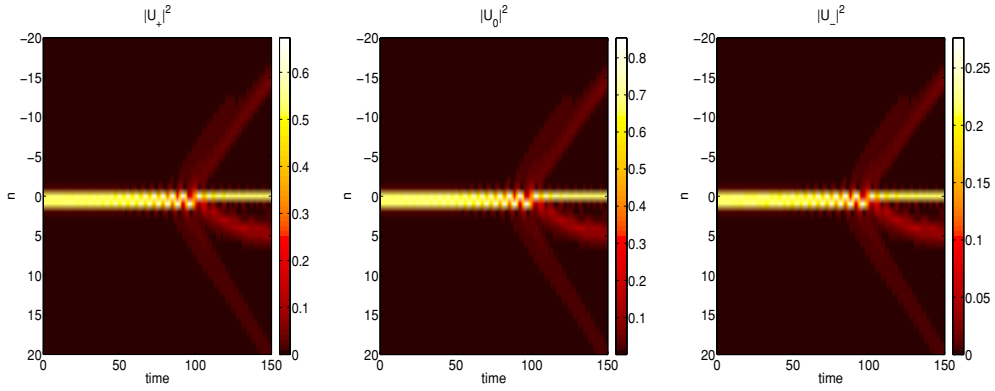

Figure 5. Spacetime contour plots of the evolution of the unstable $\ldots 00+-00\ldots$ state similarly to figure 3. The dynamics is shown for $\epsilon = 0.2$ with the weak growth rate (of the quartet of eigenvalues) illustrated in the middle right panel of figure 4 accounting for the slow and oscillatory onset of the instability.

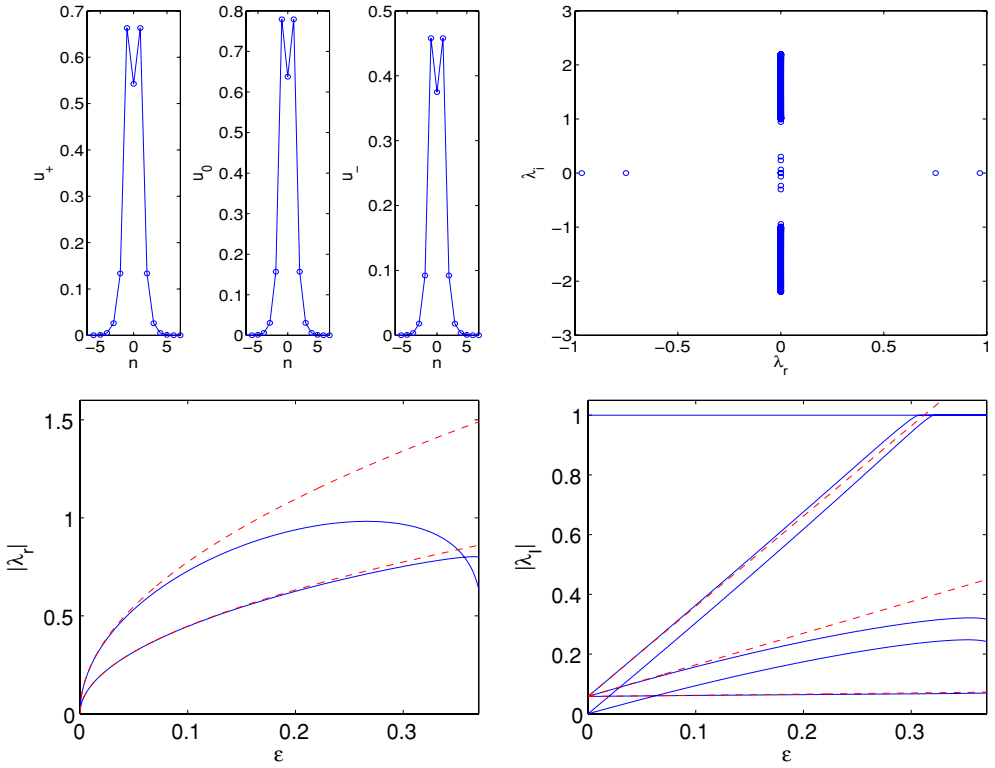

Figure 6. Similar to figure 2, this figure illustrates the three-site in-phase branch of the form $\ldots 00+++00\ldots$. The top panel represents the solution profile and its linearization eigenvalues for $\epsilon = 0.3$, while the bottom panel showcases the dependence of the eigenvalues (real and imaginary) on ϵ, comparing expressions (15) (dashed) with the numerical (solid) results.

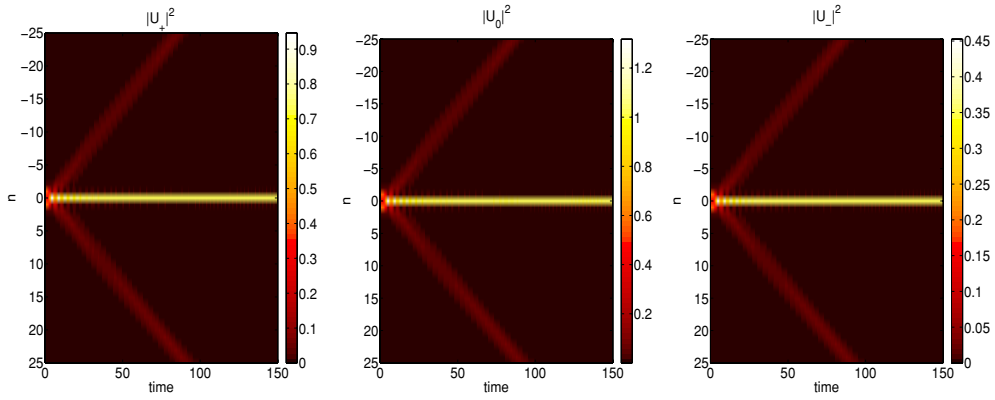

Figure 7. Similar to figure 5, but for the three-site excitation of the form $\ldots 00+++00\ldots$ and for $\epsilon = 0.3$. The fast manifestation of the instability results in the shedding of some nearly traveling at constant speed wavepackets (in both directions) and the remaining of a single-site stationary structure at the original excitation location.

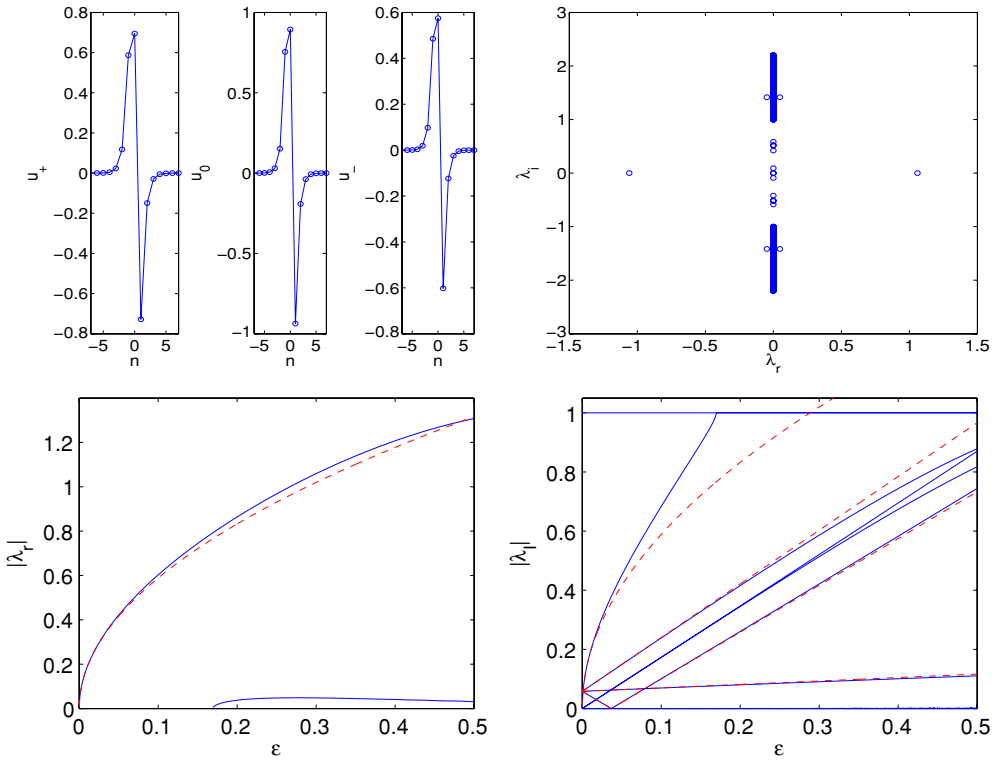

Figure 8. Same as figure 6 (also for the same value of $\epsilon = 0.3$ in the top panels) but for the configuration $\ldots 00++-00\ldots$. The solution is always unstable possessing a real eigenvalue shown in the bottom-left plot, while its corresponding imaginary eigenvalues are shown in the bottom right.

quick decomposition upon emission of smaller amplitude wavepackets, which travel at nearly constant speed through the lattice. The resulting structure is, once again, the robust single-site entity at the center location of the original three-site excitation.

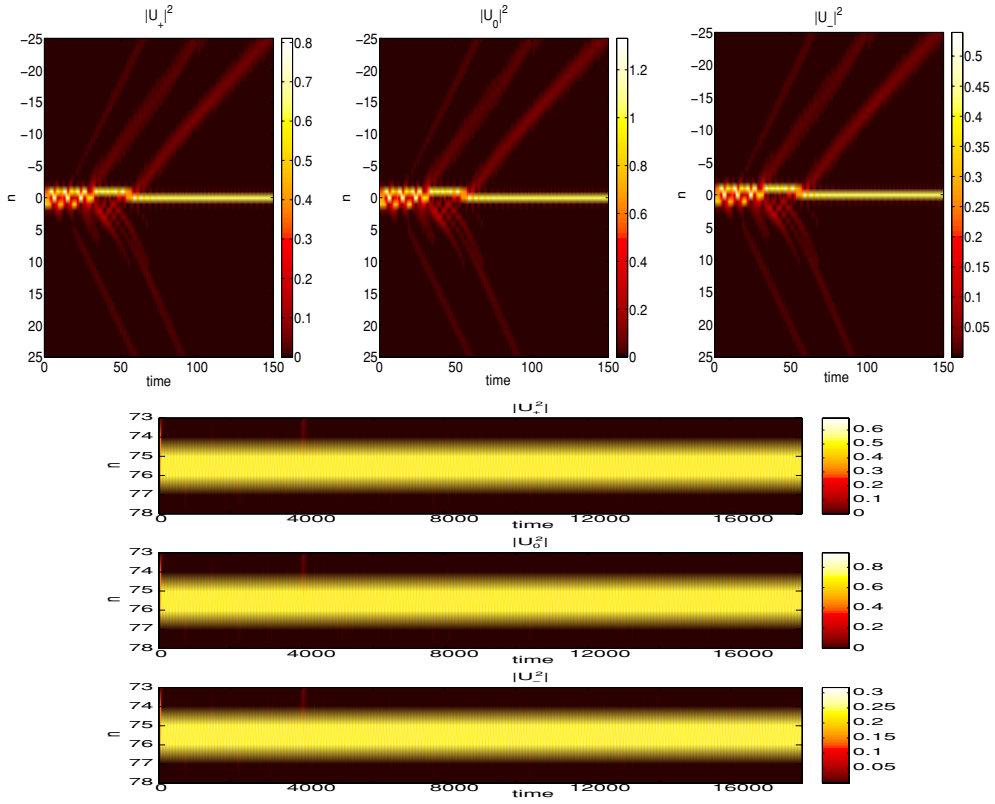

Figure 9. Same as in figure 7, but now for the . . . 00++−00 . . . excitation and $\epsilon = 0.3$ (top panels). The instabilities present through a series of emission events lead to the eventual reduction of the waveform into a single-site localized mode. In the bottom panels, the case of a lower $\epsilon = 0.129$ is shown for the same setting. In the latter case, even a two-site, out-of-phase solution is linearly stable and the evolution of the instability results in the formation of a two-site such state (rather than to the single-site one).

4.5. Three mixed-phase excited-site waveform . . . 00 + + − 00 . . .

We now turn to the configuration . . . 00 + + − 00 . . . , which features both an in-phase and an out-of-phase pair. According to the analytical predictions of equation (16), this configuration is unstable due to the presence of a real eigenvalue pair immediately bifurcating from the zero eigenvalue when the coupling constant is increased. This is confirmed in figure 8, which illustrates a typical example of the solution and its stability for $\epsilon = 0.3$. The profile shown in the figure can be continued until $\epsilon = 0.771$. As for the stability, one can note that we also obtain a very favorable comparison of the predictions of equation (16), shown through the dashed lines, with the solid lines of the full numerical results for both real and imaginary eigenvalues.

The evolution of the solution's density is shown in figure 9 illustrating an elaborate instability development. Note that this may be expected as for the value of $\epsilon = 0.3$ shown, there exists both a real and a complex eigenvalue contributing to the instability of the waveform. As a result, we observe the emission of a series of wavepackets subsequently traveling through the spinor lattice in the system, at different times. The combination of these events finally gives rise to the emergence of a robust single-site structure at the center of the original excitation.

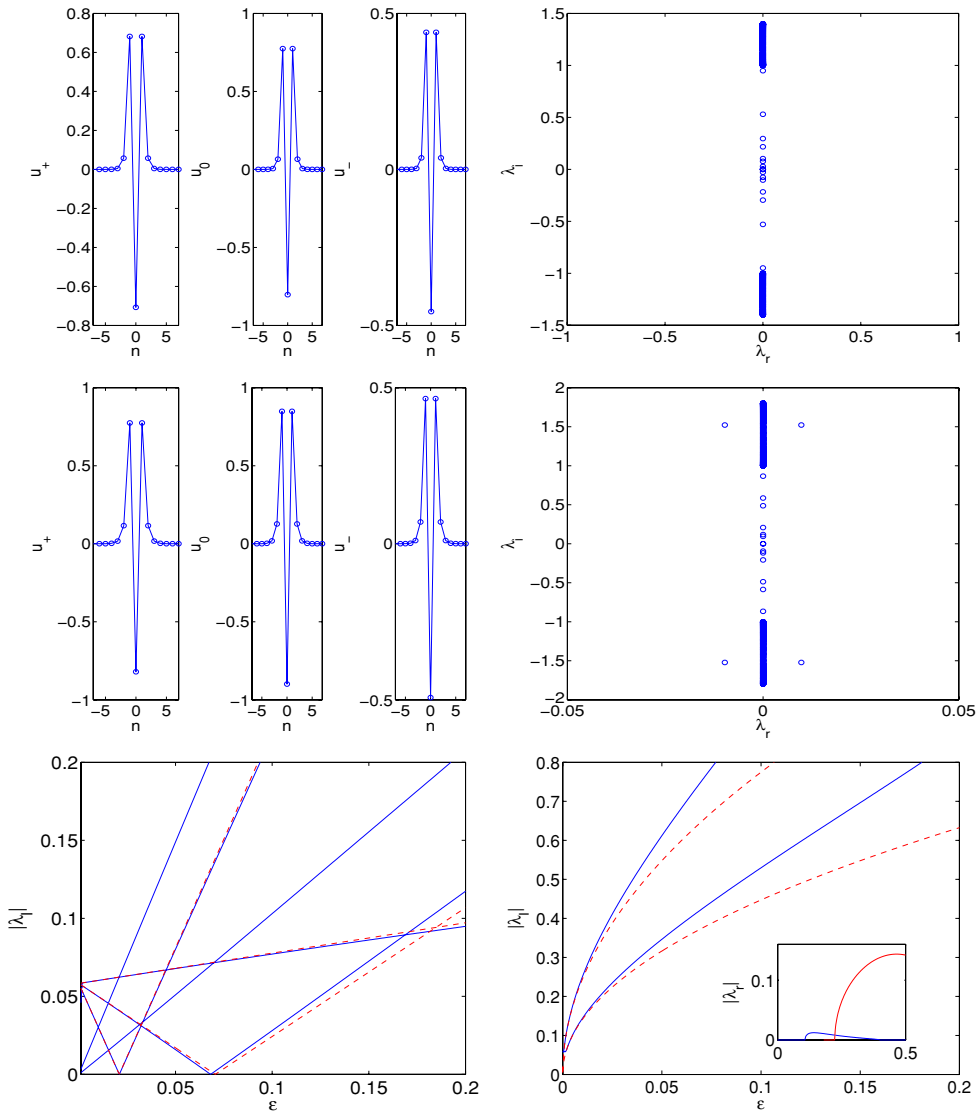

Figure 10. Similar to figure 4, but now for the configuration of the form $\ldots 00+-+00\ldots$. The top panel shows the stable case of $\epsilon = 0.1$, while the middle one is for the (oscillatorily) unstable panel of $\epsilon = 0.2$. The bottom one shows the imaginary eigenvalues as obtained numerically (solid lines) and the corresponding theoretical predictions (dashed lines). This is done for reasons of visibility in two different scales for the smaller eigenvalue pairs (one of which is at zero), shown in the left panel and for the two larger pairs of eigenvalues, shown in the right panel (the right panel also contains as an inset the real parts of the corresponding eigenvalues as they emerge due to the destabilizing collisions with the continous spectrum).

It is important to note, however, that this evolution, as a result of the development of the instability, is not the only one possible for this state. For example, within the regime of couplings of $0.108 < \epsilon < 0.147$, in addition to the single-site state, the two-site, out-of-phase configuration is also dynamically robust. Within that parameter range, we have found that it is possible that the unstable mixed-phase waveform will manifest its instability by resulting into

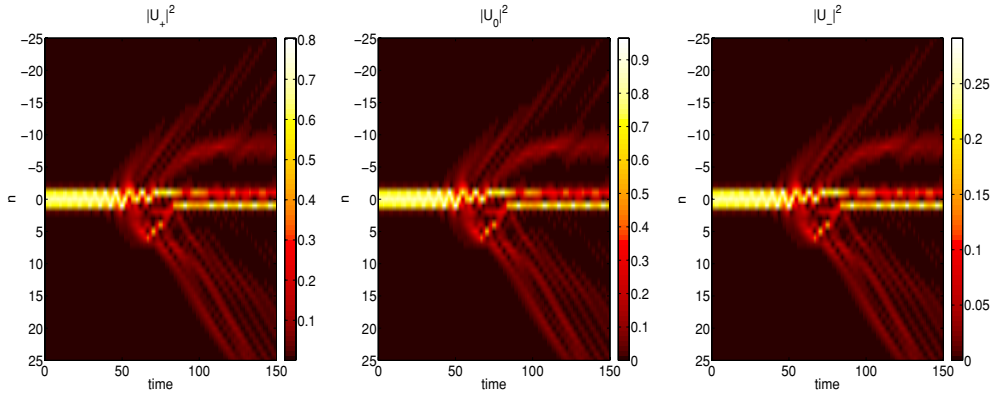

Figure 11. Spacetime contours of the dynamics of the instability manifestation for a structure of the form $\ldots 00-+-00\ldots$ for $\epsilon = 0.25$, similarly to figure 5. The oscillatory instability leads to a series of small-amplitude wavepackets emitted, eventually breaking up the structure and converting it into a two-site waveform.

an out-of-phase, two-site configuration. This possibility is highlighted in the bottom panels of figure 9.

4.6. Three out-of-phase excited-site waveform $\ldots 00+-+00\ldots$

Lastly, we consider the out-of-phase waveform containing three excited sites, which is spectrally stable for suitably small values of ϵ. In this case, even though we find that the solution becomes unstable for $\epsilon > 0.108$, it can be continued in our computations for $\epsilon < 0.747$. The relevant modes in both a stable and an unstable example for $\epsilon = 0.1$ and 0.2 are shown, respectively, in figure 10. The figure also illustrates the relevant imaginary eigenvalues as a function of ϵ, both for the smaller (left panel) and for the larger (right panel) ones among the imaginary eigenvalues, clearly showcasing the agreement with the theoretical predictions of equation (17). For the latter, the real part of the eigenvalue quartets which result from the collision of these larger imaginary eigenvalues with the continuous spectrum (and which are responsible for the instability of the solution for large values of ϵ) is shown as an inset.

In figure 11, we illustrate the dynamical evolution of the density of the three different components when $\epsilon = 0.25$. In this case, similarly to the evolution of figure 5, only oscillatory instabilities are responsible for the unstable dynamics. These generally bear a much weaker growth rate (i.e. real part), and hence the instability typically takes a longer time to develop. When it does, it is through an oscillatory growth that eventually leads to a number of different small-amplitude emission wakes. Finally, a two-site-like structure appears to persist for longer propagation distances.

5. Conclusions and future challenges

In the present work, motivated by the context of spinor BECs in optical lattices, and by the need to use analytical tools to explore the type of configurations that could be dynamically stable within that setting, we examined the nonlinear dynamical lattice variant of the corresponding continuum mean-field model. While our explorations were presented in the focusing case (of attractive interactions), they could naturally be extended to the defocusing case of repulsive interactions through the so-called staggering transformation. Our results indicated that single-site waveforms are robustly stable for all values of the tunneling between adjacent sites and

are expected to persist all the way to the continuum limit. On the other hand, for multi-site excitations, the conclusion was generalized (upon suitable calculation and detailed comparison of the eigenvalues with numerical results) that only out-of-phase excitations may be stable, while in-phase ones will always bear one or more (depending on the number of adjacent sites which are in-phase) real eigenvalue pairs. We also went on to monitor dynamically the evolution of the instabilities in the cases in which we identified the modes as unstable. Typically these led to the degeneration of the mode into a single-site excitation upon the emission of smaller amplitude wavepackets, although this was not necessarily always the case.

It would be particularly interesting to generalize the present considerations to higher dimensional settings, where additional nonlinear excitations, including ones with topological charge, are possible. In particular, it would be relevant to examine whether the discrete vortices of [20] would also preserve the stability characteristics of their single-component counterparts, as well as to explore what are potential three-dimensional excitations within this spinor system (see e.g. [19, 21] for single-component analogs). Such studies will be presented in future publications.

Acknowledgments

PGK gratefully acknowledges support from NSF-DMS-0349023 (CAREER), NSF-DMS-0806762 and from the Alexander von Humboldt Foundation.

References

[1] Stamper-Kurn D M and Ketterle W 2000 arXiv:cond-mat/0005001
[2] Stamper-Kurn D M, Andrews M R, Chikkatur A P, Inouye S, Miesner H-J, Stenger J and Ketterle W 1998 *Phys. Rev. Lett.* **80** 2027
[3] Chang M-S, Hamley C D, Barrett M D, Sauer J A, Fortier K M, Zhang W, You L and Chapman M S 2004 *Phys. Rev. Lett.* **92** 140403
[4] Stenger J, Inouye S, Stamper-Kurn D M, Miesner H-J, Chikkatur A P and Ketterle W 1998 *Nature* **396** 345
[5] Leanhardt A E, Shin Y, Kielpinski D, Pritchard D E and Ketterle W 2003 *Phys. Rev. Lett.* **90** 140403
[6] Ieda J, Miyakawa T and Wadati M 2004 *Phys. Rev. Lett.* **93** 194102
Ieda J, Miyakawa T and Wadati M 2004 *J. Phys. Soc. Japan* **73** 2996
[7] Li L, Li Z, Malomed B A, Mihalache D and Liu W M 2005 *Phys. Rev.* A **72** 033611
[8] Zhang W, Müstecaplioglu Ö E and You L 2007 *Phys. Rev.* A **75** 043601
[9] Uchiyama M, Ieda J and Wadati M 2006 *J. Phys. Soc. Japan* **75** 064002
[10] Nistazakis H E, Frantzeskakis D J, Kevrekidis P G, Malomed B A and Carretero-González R 2008 *Phys. Rev.* A **77** 033612
[11] Barnett R, Mukerjee S and Moore J E 2008 *Phys. Rev. Lett.* **100** 240405
[12] Dabrowska-Wüster B J, Ostrovskaya E A, Alexander T J and Kivshar Y S 2007 *Phys. Rev.* A **75** 023617
[13] Li Z-D and Li Q-Y 2007 *Ann. Phys.* **322** 1961
[14] Zheng G-P 2007 *J. Phys. B: At. Mol. Opt. Phys.* **40** 4493
[15] Kronjäger J, Becker C, Soltan-Panahi P, Bongs K and Sengstock K 2009 arXiv:0904.2339
[16] Becker C, Soltan-Panahi P, Kronjäger J, Dörscher S, Bongs K and Sengstock K 2009 arXiv:0912.3646
[17] Alfimov G L, Kevrekidis P G, Konotop V V and Salerno M 2002 *Phys. Rev.* E **66** 046608
[18] Pelinovsky D E, Kevrekidis P G and Frantzeskakis D J 2005 *Physica* D **212** 1
[19] Kevrekidis P G 2009 *The Discrete Nonlinear Schrödinger Equation: Mathematical Analysis, Numerical Computation and Physical Perspectives* (Heidelberg: Springer)
[20] Pelinovsky D E, Kevrekidis P G and Frantzeskakis D J 2005 *Physica* D **212** 20
[21] Lukas M, Pelinovsky D E and Kevrekidis P G 2008 *Physica* D **237** 339